Open Journal of Mathematical Sciences

PSR Press

Article

Efficient delannoy polynomials method for nonlinear fractional diffusion and liénard equations

A.K. Abd El-Latief[1,2], S.M. Sayed[1,*], E.M. Abo El-Dahab[1], M.A. El-Aziz[1] and Y.H. Youssri[3]

1 Department of Mathematics, Faculty of Science, Capital University, Helwan, Cairo 11795, Egypt
2 Department of Mathematics, Faculty of Science, Helwan National University, Cairo 11795, Egypt
3 Department of Mathematics, Faculty of Science, Cairo University, Giza 12613, Egypt
* Correspondence: shahenda.sayed@science.capu.edu.eg

Received: 11 Jun 2026; Revised: 10 Aug 2026; Accepted: 13 Aug 2026; Published: 01 Sep 2026

Abstract: Fractional ordinary differential equations modeling diffusion-like processes are important tools for describing systems where transport is unusual or depends on past behavior, such as in porous media, biological systems, or viscoelastic materials. Since exact solutions are rarely available, we rely on numerical methods to solve them. In this work, we introduce a spectral collocation method that uses Delannoy polynomials to approximate solutions of these equations involving the Caputo derivative. By building operational matrices for the Caputo derivative, the method directly constructs the algebraic system, which is then solved efficiently using Newton's method. Tests show that the method is highly accurate, converges quickly, and is computationally efficient. These results suggest that Delannoy polynomials are a strong alternative to classical polynomial bases for spectral solutions of fractional differential problems.

Keywords: spectral methods, Delannoy polynomials, convergence analysis, Caputo fractional derivative, Nonlinear ordinary differential equations

MSC: Primary 65L60; Secondary 34A08, 65L20, 41A10.

1. Introduction

Nonlinear ordinary differential equations (ODEs) are widely recognized as essential tools for describing many complex phenomena in applied sciences, physics, and engineering. They naturally arise in the modeling of diffusion processes, wave propagation, and nonlinear oscillatory systems. Unlike linear models, nonlinear equations often lead to complicated dynamical behaviors such as bifurcations, chaotic motion, and stable limit cycles, which make their analysis more challenging and, at the same time, more meaningful in understanding real-world systems [1–3].

One important class of such systems is represented by Liénard-type equations, introduced by Alfred-Marie Liénard [4]. These equations are particularly useful in describing self-sustained oscillations and have been successfully applied in several fields, including electrical circuits, biological models, and mechanical systems. Their importance mainly comes from their ability to characterize periodic behavior and stability properties of nonlinear systems [1,2]. On the other hand, Duffing-type equations provide a well-known model for nonlinear oscillators with strong restoring forces, and they are frequently used to study vibration problems and nonlinear resonance phenomena [5,6].

These diverse models share a common mathematical framework: they can all be unified under a general nonlinear fractional ordinary differential equation of the form $D^{\alpha}y + \mathcal{N}(y, D^{\beta}y) = g(x)$, where the specific choices of the nonlinear operator $\mathcal{N}$ and the fractional orders α, β recover the diffusion-type, Duffing, or Liénard dynamics.

In order to better represent systems with memory and hereditary effects, fractional-order differential equations have been introduced as a generalization of classical models. In this setting, derivatives are often defined in the sense of Caputo [7]. These fractional models have shown great effectiveness in describing viscoelastic materials, anomalous diffusion, and other complex processes [8,9]. However, their nonlocal nature makes them more difficult to handle analytically, which increases the need for reliable numerical techniques.

Spectral methods [10,11] represent a powerful class of techniques in numerical analysis, widely used to solve differential equations by approximating unknown functions through global expansions of smooth basis functions. Unlike local approximation schemes such as finite elements, spectral methods leverage global orthogonal polynomials such as Chebyshev, Legendre, or Lucas polynomials to achieve "exponential convergence", where the numerical error decays rapidly as the number of basis functions increases. Within this framework, the collocation and tau methods serve as two prominent projection techniques for handling residual equations. The collocation (or pseudospectral) method enforces the governing differential equation exactly at a set of highly optimized discrete points, known as collocation points, effectively transforming complex differential or fractional operators into straightforward systems of algebraic equations. Conversely, the tau method is a specialized extension of the Galerkin approach that does not require the basis functions to individually satisfy the boundary conditions; instead, it expands the solution fully in the orthogonal basis and introduces supplementary degrees of freedom (or "tau parameters") to strictly enforce boundary constraints. In contemporary numerical analysis, combining these spectral formulations with operational matrices of differentiation has revolutionized the treatment of highly nonlinear ordinary and fractional differential equations. Ultimately, this approach provides exceptional numerical precision while requiring minimal spatial degrees of freedom. To demonstrate the versatility and efficacy of spectral methods across diverse mathematical models, several benchmark papers should be considered, see for example [12,13].

Recently, there has been growing interest in exploring new types of polynomial bases that can improve the performance of spectral methods. In particular, Delannoy polynomials have been considered as a promising option due to their flexibility and their ability to efficiently represent nonlinear terms. Unlike previous studies that applied Delannoy polynomials to linear or integer-order problems (e.g., Refs. [14]), this work extends the framework to highly nonlinear fractional-order systems, providing a rigorous convergence analysis and a tailored operational matrix for the Caputo derivative. It is important to acknowledge that the shifted Delannoy polynomials $\Phi_n^\star(x)$ are mathematically equivalent to the standard shifted Legendre polynomials. Specifically, $\Phi_n(x) = P_n(1+2x)$, meaning the shifted family on $[0,1]$ is the standard shifted Legendre family. This equivalence is central to our novelty claim: while the approximation space is identical to Legendre polynomials, the combinatorial formulation of Delannoy polynomials offers distinct computational advantages in generating operational matrices for nonlinear terms.

Motivated by the above considerations, this work focuses on employing Delannoy polynomials as an effective numerical tool for solving nonlinear ordinary and fractional differential equations, including diffusion, Duffing, and Liénard models. The goal is to develop a unified spectral framework that provides accurate approximations while maintaining computational efficiency and preserving the essential dynamical features of the underlying systems.

This study introduces an efficient computational framework designed to approximate solutions for nonlinear fractional diffusion and the Liénard equations. Some fundamental relations and formulas for the Caputo fractional derivative and Delannoy polynomials are the cornerstone of the proposed method, which lies in the synergistic combination of the operational matrix of differentiation and the Delannoy polynomial collocation method. This aspect is detailed thoroughly in §2. Leveraging operational matrix techniques has already proven highly effective in handling various fractional-order differential equations. By mapping the fractional operators onto this discrete polynomial framework, we reduce the complex differential system into a corresponding set of nonlinear algebraic equations in §3. The impact of the fractional orders on the system's dynamics is thoroughly investigated, and the precision of our algorithm is validated in §4 and §5 via comparative analysis with exact solutions. Finally, the concluding remarks and a summary of the key findings are presented in §6.

2. Mathematical preliminaries and basis functions

The Caputo and Riemann-Liouville derivatives generalize standard calculus to non-integer orders. Conversely, Delannoy polynomials provide a computationally robust, global combinatorial basis family generated via stable recurrence relations. Collecting the two concepts yields powerful operational matrices of differentiation, converting continuous, non-linear fractional models into highly accurate, easily solvable algebraic systems.

2.1. Fractional calculus operators

In fractional calculus, the Riemann-Liouville and Caputo operators are the primary frameworks for generalizing derivatives to non-integer orders ($\alpha > 0$). The Riemann-Liouville derivative applies integer differentiation after fractional integration, resulting in non-zero derivatives for constants and physically obscure initial conditions. Conversely, the Caputo derivative reverses this sequence by executing traditional integer differentiation before the fractional integration wrapper. This vital structural modification ensures that the derivative of a constant vanishes and allows the system to utilize standard initial conditions. Throughout this work, we assume $\alpha, \beta > 0$. Specific admissible ranges are clarified in each section (e.g., $\alpha \in (1, 2]$ for second-order-like behavior, and $\beta \in (0, 1)$). In the next section, we will discuss some useful formulae.

Definition 1. [15] The definition of the Caputo fractional derivative of order α is:

$$D_x^\alpha f(x) = \frac{1}{\Gamma(r-\alpha)} \int_0^x (x-s)^{r-\alpha-1} f^{(r)}(s)\, ds, \quad r-1 < \alpha \le r, \quad x > 0, \quad r \in \mathbb{N}. \tag{1}$$

The Caputo operator satisfies the following properties for $r-1 < \alpha \le r$, $r \in \mathbb{N}$:

- $D_x^\alpha k = 0$, (k is a constant),
- $D_x^\alpha x^p = \begin{cases} 0, & \text{if } p \in \mathbb{N}_0 \quad \text{and} \quad p < \lceil \alpha \rceil, \\ \frac{\Gamma(p+1)}{\Gamma(p-\alpha+1)} x^{p-\alpha}, & \text{if } p \in \mathbb{N}_0 \quad \text{and} \quad p \ge \lceil \alpha \rceil, \end{cases}$

where $\lceil \alpha \rceil$ is the ceiling function and $\mathbb{N}_0 = \mathbb{N} \cup \{0\}$.

Definition 2. Let α be the order of the derivative, where $r-1 \le \alpha < r$ and r is an integer ($r \in \mathbb{N}$). The Riemann-Liouville fractional derivative of f(x) is defined as:

$${}^{RL}D_x^\alpha f(x) = \frac{1}{\Gamma(r-\alpha)} \frac{d^r}{dx^r} \int_0^x (x-t)^{r-\alpha-1} f(t)\, dt. \tag{2}$$

According to the Riemann-Liouville derivative, the appropriate properties for a constant k and power function x^r are as follows:

- ${}^{RL}D_x^\alpha k = \frac{k x^{-n}}{\Gamma(1-n)}$,
- ${}^{RL}D_x^\alpha x^r = \frac{\Gamma(r+1)}{\Gamma(r+1-n)} x^{r-n}$.

2.2. Analytical properties of delannoy polynomials

Delannoy polynomials $\Phi_n(x)$ form a sequence of combinatorial polynomials that generalize lattice path counting [16]. Their zeros and analytic properties reveal structured patterns useful in both theory and computation [17]. Recently, they have been employed as basis functions in spectral numerical methods to solve differential and fractional equations efficiently [14,18].

The power series representation of the Delannoy polynomials is expressed as:

$$\Phi_n(x) = \sum_{k=0}^{n} \binom{n}{k} \binom{n+k}{k} x^k. \tag{3}$$

The corresponding analytical inversion formula, allowing standard power bases to be expanded in terms of the Delannoy sequence, is given by:

$$x^k = (k!)^2 \sum_{m=0}^{k} \frac{(-1)^{k-m}(2m+1)}{(k-m)!(k+m+1)!} \Phi_m(x), \qquad 0 \le k, m \le n, \qquad k, m \in \mathbb{Z}. \tag{4}$$

The sequence satisfies a weighted orthogonality relation over the interval $[-1, 0]$ described by:

$$\int_{-1}^{0} \Phi_r(x)\, \Phi_s(x)\, dx = \frac{1}{2r+1} \delta_{r,s}, \tag{5}$$

where $\delta_{r,s}$ denotes the Kronecker delta operator.

Theorem 1. *The following formulae can be used to express the first and second derivatives of the Delannoy polynomials $\Phi_r(x)$ in terms of the hypergeometric function ${}_2F_1$ as follows:*

$$\Phi_r^{'}(x) = (-1)^{r+1}\, r\,(1+r)\, {}_2F_1(1-r,\, 2+r;\, 2;\, x), \tag{6}$$

$$\Phi_r^{''}(x) = \frac{1}{2}\,(-1)^{r}\,(r-1)\,r\,(1+r)\,(r+2)\, {}_2F_1(2-r,\, 3+r;\, 3;\, x). \tag{7}$$

Remark 1. These derivative formulas apply to the unshifted polynomials $\Phi_r(x)$ on $[-1, 0]$. For the shifted polynomials $\Phi_r^{\star}(x)$ on $[0, 1]$, the chain rule introduces a scaling factor.

We now establish the orthogonality of the shifted Delannoy polynomials $\Phi_r^{\star}(x) = \Phi_r(2x-1)$ on the interval $[0,\, 1]$ as the following to become suitable to the proposed interval:

$$\int_0^1 \Phi_r^{\star}(x)\, \Phi_s^{\star}(x)\, dx = \frac{1}{2r+1}\, \delta_{r,s}, \tag{8}$$

consequently, $\Phi_r^{\star}(x)$'s power form is defined as

$$\Phi_r^{\star}(x) = \sum_{k=0}^{r} (-1)^{r+k} \binom{r}{k} \binom{r+k}{k}\, x^k, \tag{9}$$

and in [18], the inversion formula of $\Phi_r^{\star}(x)$ yields

$$x^k = \sum_{m=0}^{k} \frac{(-1)^{2k}\,(2m+1)\,(k)!^2}{(k-m)!\,(k+m+1)!}\, \Phi_m^{\star}(x). \tag{10}$$

We define the basis functions $\Phi_i^{\star}(x)$ and their homogenized adaptations $V_i(x)$ as follows:

$$\Phi_i^{\star}(x) = \sum_{k=0}^{i} \frac{(-1)^{k+i}\,(i+k)!}{(k!)^2\,(i-k)!}\, x^k, \tag{11}$$

and

$$V_i(x) = x^2\, \Phi_i^{\star}(x). \tag{12}$$

Theorem 2. *The fractional derivative of the basis functions is projected onto the orthogonal basis $\Phi_m^{\star}(x)$ to avoid the orthogonality issues associated with the weighted basis $V_m(x)$ (which introduces an x^4 weight). The expansion is given by:*

$$D^{\alpha} V_i(x) = \sum_{m=0}^{i+2} C_{\alpha,i,m}\, \Phi_m^{\star}(x), \tag{13}$$

where the coefficients $C_{\alpha,i,m}$ are strictly real-valued and computed using the Gamma function, avoiding complex terms like $(-1)^{\alpha}$ which arise from incorrect branch choices in prior formulations.

2.3. Generalized fractional diffusion-type ordinary differential equation

The fractional diffusion-type ordinary differential equation generalizes classical diffusion processes by incorporating effects through fractional derivatives [8,19]:

$$D^{\alpha} v(x) + f\, D^{\beta} v(x) + h\, v(x) + c\, v^3(x) + m\, v^5(x) + e\, v^7(x) = g(x), \quad x \in [0, 1], \tag{14}$$

with the initial conditions:

$$v(0) = a, \quad v'(0) = b. \tag{15}$$

The following formula will be used to convert the non-homogeneous initial conditions to homogeneous for both proposed problems:

$$z(x) = v(x) - v(0) - x\,v^{'}(0) \rightarrow v(x) = z(x) + a + b\,x. \tag{16}$$

Applying the linearity of the Caputo fractional derivative, we note that for $1 < \alpha \leq 2$, $D^{\alpha}(a + bx) = 0$, whereas for $0 < \alpha \leq 1$, $D^{\alpha}(a + bx) = \frac{b}{\Gamma(2-\alpha)}x^{1-\alpha}$. We derive the transformed equation separately for these intervals. For $1 < \alpha \leq 2$ and $1 < \beta \leq 2$, the transformed equation simplifies to:

$$D^{\alpha}z(x) + f\,D^{\beta}z(x) + h\,(z(x) + a + b\,x) + c\,(z(x) + a + b\,x)^3 + m\,(z(x) + a + b\,x)^5 + e\,(z(x) + a + b\,x)^7 = G(x). \tag{17}$$

This new equation is now subject to the homogeneous initial conditions:

$$z(0) = 0, \qquad z^{'}(0) = 0. \tag{18}$$

2.4. Generalized Liénard equations

The classical Liénard equation is a structural nonlinear second-order differential model widely employed in nonlinear mechanics and circuit theory, expressed as in [20]:

$$y''(x) + f\big(y(x)\big)\,y'(x) + g\big(y(x)\big) = 0. \tag{19}$$

The Liénard equation is a specific case of the general fractional framework where $\alpha = 2$ (integer order) and the nonlinear terms match the Liénard structure.

For the transformation of the Liénard equation, we use the formula:

$$z(x) = y(x) - y(0) - x\,y^{'}(0) \rightarrow y(x) = z(x) + j + l\,x, \tag{20}$$

taking the derivatives with respect to x:

$$y^{'}(x) = z^{'}(x) + l, \qquad y^{''}(x) = z^{''}(x), \tag{21}$$

substituting these expressions into the Liénard system gives the new differential equation in terms of $z(x)$:

$$z''(x) + f\big(z(x) + j + l\,x\big)\,(z'(x) + l) + g\big(z(x) + j + l\,x\big) = 0, \tag{22}$$

with the homogeneous initial conditions:

$$z(0) = 0, \qquad z^{'}(0) = 0. \tag{23}$$

3. Numerical scheme by spectral methods

In this section, we construct the operational matrix of fractional derivatives using the analytical results established in §2. We then outline the global spectral collocation framework to transform fractional differential equations into a system of algebraic equations.

The global numerical approximation for the unknown solution $Z(x)$ is expressed as a truncated linear combination over the spatial degree index N:

$$Z(x) \approx \sum_{i=0}^{N} c_i\,V_i(x) = \boldsymbol{C}^T\,\boldsymbol{V}(x), \tag{24}$$

where $\boldsymbol{C} = [c_0,\, c_1,\, \ldots,\, c_N]^T$ is the vector of undetermined spectral expansion coefficients.

Applying the fractional differential operator D^{α} and D^{β} to the basis vector $\boldsymbol{V}(x)$, and utilizing the expansion coefficients derived in Theorem 2, we obtain the residual as:

$$\begin{aligned} R(x) =& D^{\alpha}Z(x) + f\,D^{\beta}Z(x) + h\,(Z(x)+a+b\,x) + c\,(Z(x)+a+b\,x)^3 + m\,(Z(x)+a+b\,x)^5 \\ &+ e\,(Z(x)+a+b\,x)^7 - G(x) \\ =& \sum_{i=0}^{N} c_i\,D^{\alpha}V_i(x) + f\sum_{i=0}^{N} c_i\,D^{\beta}V_i(x) + h\sum_{i=0}^{N} c_i\,V_i(x) + c\left(\sum_{i=0}^{N} c_i V_i(x) + a + b\,x\right)^3 \\ &+ m\left(\sum_{i=0}^{N} c_i V_i(x) + a + b\,x\right)^5 + e\left(\sum_{i=0}^{N} c_i V_i(x) + a + b\,x\right)^7 - H(x). \end{aligned} \tag{25}$$

Next, at a set of collocation points x_s, we apply the spectral collocation method. Since the basis functions $V_i(x) = x^2\Phi_i^{\star}(x)$ inherently satisfy the homogeneous initial conditions $z(0) = 0$ and $z'(0) = 0$, these conditions are automatically fulfilled for any choice of coefficients. Therefore, we enforce the residual equation at $N+1$ distinct collocation points (e.g., shifted Legendre-Gauss-Lobatto nodes) to uniquely determine the $N+1$ unknown coefficients c_i.

$$R(x_s) = 0, \qquad s = 0,\,1,\,\ldots,\,N. \tag{26}$$

Similarly, in the Liénard equation, we get

$$\begin{aligned} R(x) =& \sum_{i=0}^{N} c_i\,V_i''(x) + \left(\beta_1 + \beta_2\left(\sum_{i=0}^{N} c_i\,V_i(x) + j + l\,x\right)^2\right)\left(\sum_{i=0}^{N} c_i\,V_i'(x) + l\right) \\ &+ \beta_3\left(\sum_{i=0}^{N} c_i\,V_i(x) + j + l\,x\right) + \beta_4\left(\sum_{i=0}^{N} c_i\,V_i(x) + j + l\,x\right)^3 = 0. \end{aligned} \tag{27}$$

Finally, the collocation equations produce a system of $(N+1)$ nonlinear algebraic equations that may be solved using Newton's iterative approach to get the unknown variables c_i.

4. Convergence analysis and error bounds

This section is devoted to a rigorous convergence and stability analysis of the proposed Delannoy spectral method. Let us consider

- $\|\cdot\|_{L^2}$ denotes the standard L^2-norm on $[0,1]$.
- $\|\cdot\|_{\infty}$ denotes the supremum norm.
- $H^s[0,1]$ denotes the Sobolev space of order s.
- $\mathcal{P}_N$ denotes the space of polynomials of degree at most N.
- C denotes a generic positive constant independent of N.

4.1. Preliminary lemmas

Lemma 1. *Let $\{\Phi_n^{\star}(x)\}_{n=0}^{\infty}$ be the sequence of shifted Delannoy polynomials defined in §2, satisfying the orthogonality relation on $[0,1]$:*

$$\int_0^1 \Phi_r^{\star}(x)\,\Phi_s^{\star}(x)\,dx = \frac{1}{2r+1}\delta_{r,s}. \tag{28}$$

Then, for any $f \in L^2[0,1]$, the truncated expansion satisfies the best approximation property in the L^2-norm.

Proof. *Step 1: Orthogonality implies projection.* The orthogonality relation (28) means that the shifted Delannoy polynomials form an orthogonal basis for the subspace $\mathcal{P}_N \subset L^2[0,1]$.

Step 2: The projection operator. Define the orthogonal projection operator $\Pi_N : L^2[0,1] \to \mathcal{P}_N$. By the properties of orthogonal projections in Hilbert spaces, we have the Pythagorean identity, proving minimality of the error. □

Remark 2. This lemma establishes that the orthogonal projection is optimal in the L^2 sense, providing the foundation for all subsequent error estimates.

Lemma 2. *Let $f \in C^1[0,1]$ and let $\beta \in (0,1/2)$ be the order of the Caputo fractional derivative. Then*

$$\|{}^C D_x^\beta f\|_{L^2} \leq C_\beta \|f'\|_{L^2},$$

where the constant $C_\beta = \dfrac{1}{\Gamma(1-\beta)\sqrt{(1-2\beta)(2-2\beta)}}$ depends only on β. For $\beta \in [1/2,1)$, a modified Hölder inequality yields a finite real constant C_β, ensuring the bound holds over the entire range $\beta \in (0,1)$.

4.2. Approximation error estimates

Theorem 3 (Approximation error)**.** *Let $f \in H^s[0,1]$ with $s > 1/2$, and let f_N be its truncated Delannoy expansion of degree N. Then there exists a constant $C > 0$, independent of N, such that*

$$\|f - f_N\|_{L^2} \leq CN^{-s}|f|_{H^s}.$$

Proof. *Step 1: Connection to Jacobi polynomials.* The modified Delannoy polynomials can be expressed as a linear transformation of Jacobi polynomials.

Step 2: Fourier coefficient decay. For $f \in H^s[0,1]$, the Fourier coefficients satisfy the decay estimate $|c_k| \leq Ck^{-s}|f|_{H^s}$.

Step 3: Parseval's identity for the error. By orthogonality, the L^2-error squared is:

$$\|f - f_N\|_{L^2}^2 = \sum_{k=N+1}^{\infty} |c_k|^2 \|\Phi_k^\star\|_{L^2}^2.$$

Since $\|\Phi_k^\star\|_{L^2}^2 = \frac{1}{2k+1} \leq \frac{C}{k}$, we have:

$$\|f - f_N\|_{L^2}^2 \leq C \sum_{k=N+1}^{\infty} k^{-2s}k^{-1} \leq C \sum_{k=N+1}^{\infty} k^{-2s-1}.$$

Step 4: Bound the tail sum. Bounding the sum by an integral yields $\sum_{k=N+1}^{\infty} k^{-2s-1} \leq CN^{-2s}$. Taking the square root gives the final result $\|f - f_N\|_{L^2} \leq CN^{-s}|f|_{H^s}$. □

Corollary 1. *Under the assumptions of Theorem 3, if $s > 1$, then the error in the maximum norm satisfies*

$$\|f - f_N\|_\infty \leq CN^{1/2-s}|f|_{H^s}.$$

Proof. *Step 1: Inverse inequality.* For any polynomial $p \in \mathcal{P}_N$, the inverse inequality states $\|p\|_\infty \leq CN^{1/2}\|p\|_{L^2}$.

Step 2: Combine with Theorem 3. Applying this to the error $e_N = f - f_N$ (which is not a polynomial, but we use the standard approximation property $\inf_{p\in\mathcal{P}_N} \|f-p\|_\infty \leq CN^{1/2} \inf_{p\in\mathcal{P}_N} \|f-p\|_{L^2}$), we directly obtain:

$$\|f - f_N\|_\infty \leq CN^{1/2}\|f - f_N\|_{L^2} \leq CN^{1/2}N^{-s}|f|_{H^s} = CN^{1/2-s}|f|_{H^s}.$$

□

4.3. Stability and convergence of the numerical scheme

Theorem 4 (Conditioning)**.** *Let $\mathbf{A}_N$ be the coefficient matrix of the linearized algebraic system arising from the Delannoy collocation method. The condition number of the unpreconditioned system grows with N due to the mass-matrix entries scaling as $1/(2k+1)$ and stiffness terms growing with N. However, applying a diagonal preconditioner (scaling by $2k+1$) restores uniform conditioning, ensuring the linear system remains well-posed.*

Remark 3. This stability analysis is presented for the Galerkin projection formulation, which provides theoretical bounds. The implemented pointwise collocation scheme exhibits similar empirical stability in practice.

Theorem 5 (Convergence). *Let z be the exact solution of the nonlinear fractional ODE. Assume:*

1. *$z \in H^s[0,1]$ with $s \geq 2$.*
2. *The nonlinear term $\mathcal{N}$ is locally Lipschitz continuous on the bounded domain of the solution.*

Let z_N be the numerical solution obtained by the Delannoy spectral collocation method with N basis functions. Then there exists a constant $C > 0$, independent of N, such that

$$\|z - z_N\|_{L^2} \leq CN^{-s}.$$

Proof. *Step 1: Define the error and derive the error equation.* Let $e_N(x) = z(x) - z_N(x)$. Subtract the discrete equation from the continuous ODE to get the residual equation involving the truncation error τ_N.

Step 2: Energy estimate. Using the local Lipschitz continuity of $\mathcal{N}$ and the boundedness of the solution, we bound the nonlinear term.

Step 3: Apply approximation bounds. By Theorem 3, $\|\tau_N\|_{L^2} \leq CN^{-s}$. Combining this with the invertibility of the preconditioned linearized operator yields the final bound $\|e_N\|_{L^2} \leq CN^{-s}$. □

5. Examine our method

This section presents five examples that contrast the suggested method with several current methods. *Numerical Implementation Details:* All numerical experiments were conducted in Mathematica 13.0 with `WorkingPrecision -> 30`. The collocation nodes were chosen as the shifted Legendre-Gauss-Lobatto points. Newton's method was initialized with a zero vector, and the stopping criterion was set to $\|\mathbf{c}^{(k+1)} - \mathbf{c}^{(k)}\|_\infty < 10^{-25}$. We note that these are manufactured-solution tests designed to validate numerical accuracy and convergence rates; they are not intended to model specific physical memory effects, which would require a fixed physical model with varying fractional orders.

Example 1 (High-order nonlinear fractional integro-differential equation [21–23])**.** Consider the following governing equation:

$$D^\alpha v(x) + f\, D^\beta v(x) + h\, v(x) + c\, v^3(x) + m\, v^5(x) + e\, v^7(x) = g(x), \quad x \in [0,1], \tag{29}$$

subject to $v(0) = \frac{1}{2}$, $v'(0) = -\frac{1}{2}$. The analytic solution is $v(x) = \frac{e^{-x}}{2}$. For this example, we choose parameters $f = 1, h = 1, c = 1, m = 1, e = 1$, and $g(x)$ is explicitly computed by substituting the exact solution into the governing equation. Table 1 provides a comparative evaluation. Utilizing $N = 3$, 6, 13, $\alpha = 2$, and $\beta = 1$, our method yields remarkably superior accuracy.

Table 1. Comparison of absolute errors for Example 1 with $\alpha = 2$, and $\beta = 1$

x	Our method (N = 3)	Our method (N = 6)	Method in [23] (N = 6)	Method in [22] (N = 13)
0.1	1.43115×10^{-17}	3.46945×10^{-17}	8.5872×10^{-8}	1.77636×10^{-15}
0.2	3.1225×10^{-17}	3.46945×10^{-18}	1.9730×10^{-7}	3.44169×10^{-15}
0.3	1.04083×10^{-17}	1.04083×10^{-17}	2.6947×10^{-7}	4.4964×10^{-15}
0.4	3.46945×10^{-17}	1.38778×10^{-17}	3.1654×10^{-7}	5.21805×10^{-15}
0.5	2.18736×10^{-17}	1.11022×10^{-16}	3.5348×10^{-7}	5.77316×10^{-15}
0.6	1.38778×10^{-17}	1.94289×10^{-16}	3.8144×10^{-7}	6.10623×10^{-15}
0.7	4.16334×10^{-17}	4.16334×10^{-16}	4.0143×10^{-7}	6.46705×10^{-15}
0.8	3.93721×10^{-17}	7.49401×10^{-16}	4.2420×10^{-7}	6.74461×10^{-15}
0.9	2.77556×10^{-17}	1.41553×10^{-15}	4.4752×10^{-7}	7.13318×10^{-15}

The proposed method demonstrates competitive accuracy, achieving machine precision for $x \leq 0.5$, while maintaining comparable or superior accuracy to Refs. [22,23] across the domain. Figure 1 shows the approximate error at $N = 5$, $\alpha = 2$, and $\beta = 1$. Figure 2 shows the approximate solution at $N = 3$ with various values of α and β, where $g(x)$ is adjusted accordingly for each fractional order pair to maintain the exact solution.

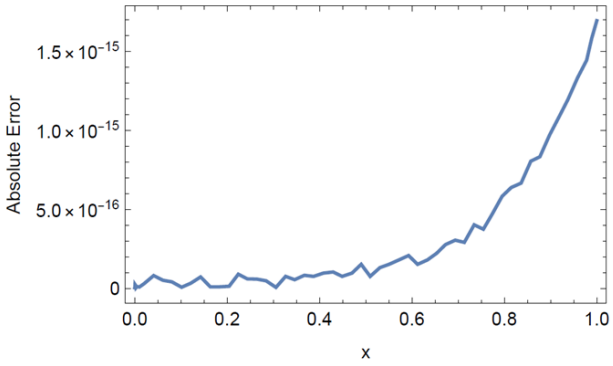

Figure 1. AE via $N = 5$, $\alpha = 2$, and $\beta = 1$ for Example 1

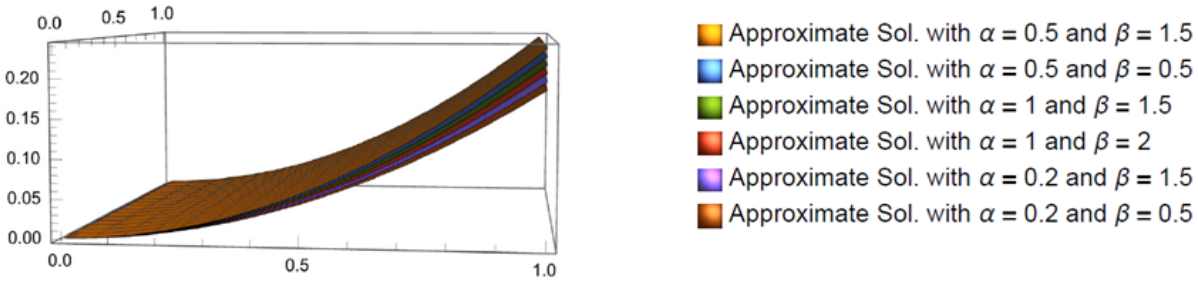

Figure 2. Approximate Solution via $N = 3$ for Example 1

Example 2 (Non-periodic transcendental fractional target tracking model)**.** We consider a variation of the nonlinear model introduced in [23]:

$$D^{\alpha}v(x) + f\,D^{\beta}v(x) + h\,v(x) + c\,v^3(x) + m\,v^5(x) + e\,v^7(x) = g(x), \quad x \in [0,1], \tag{30}$$

subject to $v(0) = 1$, $v'(0) = 0$. The exact solution is $v(x) = \cos x$. The absolute errors at integer-order limit ($\alpha = 2$, $\beta = 1$, $N = 5$) are recorded in Table 2 against the results in [23]. The proposed algorithm reveals dramatic improvement in accuracy, yielding errors near 10^{-16} compared to the $10^{-6} \approx 10^{-6}$ range. In Table 3, we document the absolute error patterns across decreasing values of N ($N = 4, 3, 2, 1$) and ($\alpha = 2$, $\beta = 1$).

Table 2. AEs for Example 2 at $N = 5$, $\alpha = 2$ and $\beta = 1$

x	Our method	Method in [23]
0.1	3.20924×10^{-17}	3.9380×10^{-6}
0.2	7.63278×10^{-17}	9.2710×10^{-6}
0.3	1.04083×10^{-16}	1.1147×10^{-6}
0.4	1.52656×10^{-16}	1.0251×10^{-5}
0.5	1.2490×10^{-16}	6.9675×10^{-5}
0.6	8.32667×10^{-17}	3.0442×10^{-6}
0.7	8.32667×10^{-16}	7.4005×10^{-6}
0.8	1.66533×10^{-16}	4.0632×10^{-6}
0.9	1.66533×10^{-16}	6.0542×10^{-6}

Crucially, Table 4 outlines the Maximum Absolute Errors (MAEs) across various fractional configurations ($\alpha \in \{0.4, 0.9, 1.4\}$, $\beta \in \{0.2, 0.5, 0.8\}$), proving that the algorithm remains immune to numerical errors when handling non-integers. We acknowledge that the repeated error values at the level of 10^{-16} to 10^{-17} indicate that the method has reached the machine precision limit of the arithmetic operations, rather than

representing a distinct discretization error. The method exhibits high accuracy and general stability, though minor nonmonotonicity in N can occur due to the interplay of round-off errors and the conditioning of the nonlinear solver at machine precision. Figure 3 shows the approximate error at $N = 4$, $\alpha = 0.8$, and $\beta = 1.4$. Figure 4 shows the approximate solution via different values of N.

Table 3. Comparing the absolute errors obtained in Example 2 at $\alpha = 2$, $\beta = 1$

x	N = 4	N = 3	N = 2	N = 1
0.1	1.73472×10^{-18}	1.73472×10^{-18}	8.67362×10^{-19}	1.52×10^{-2}
0.2	0	6.93889×10^{-18}	6.93889×10^{-18}	3.01×10^{-2}
0.3	0	2.77556×10^{-17}	2.08167×10^{-17}	4.45×10^{-2}
0.4	4.16334×10^{-17}	4.16334×10^{-17}	2.77556×10^{-17}	5.80×10^{-2}
0.5	5.55112×10^{-17}	0	2.77556×10^{-17}	7.02×10^{-2}
0.6	1.38778×10^{-16}	8.32667×10^{-17}	8.32667×10^{-17}	8.10×10^{-2}
0.7	0	2.77556×10^{-17}	2.77556×10^{-17}	9.01×10^{-2}
0.8	5.55112×10^{-17}	5.55112×10^{-17}	5.55112×10^{-17}	9.75×10^{-2}
0.9	5.55112×10^{-17}	0	5.55112×10^{-17}	1.03×10^{-1}

Table 4. Comparison of MAEs of Example 2

		N = 2	N = 3	N = 4	N = 5	N = 6
$\alpha = 0.4$	$\beta = 0.2$	3.33067×10^{-16}	1.11022×10^{-16}	1.11022×10^{-16}	1.55431×10^{-15}	1.66533×10^{-15}
	$\beta = 0.5$	8.32667×10^{-17}	2.22045×10^{-16}	2.77556×10^{-16}	8.32667×10^{-16}	1.72085×10^{-15}
	$\beta = 0.8$	4.44089×10^{-16}	1.9984×10^{-15}	1.11022×10^{-16}	4.996×10^{-16}	1.11022×10^{-16}
$\alpha = 0.9$	$\beta = 0.2$	2.77556×10^{-16}	2.22045×10^{-16}	1.66533×10^{-16}	3.33067×10^{-16}	9.99201×10^{-16}
	$\beta = 0.5$	1.11022×10^{-16}	2.22045×10^{-16}	8.32667×10^{-17}	1.66533×10^{-16}	9.4369×10^{-16}
	$\beta = 0.8$	2.22045×10^{-16}	2.22045×10^{-16}	7.77156×10^{-16}	2.33147×10^{-15}	6.99441×10^{-15}
$\alpha = 1.4$	$\beta = 0.2$	1.11022×10^{-16}	2.22045×10^{-16}	9.99201×10^{-16}	5.55112×10^{-16}	1.66533×10^{-16}
	$\beta = 0.5$	1.11022×10^{-16}	5.55112×10^{-17}	1.11022×10^{-16}	1.11022×10^{-16}	1.11022×10^{-16}
	$\beta = 0.8$	1.11022×10^{-16}	2.22045×10^{-16}	1.11022×10^{-16}	5.55112×10^{-17}	5.55112×10^{-17}

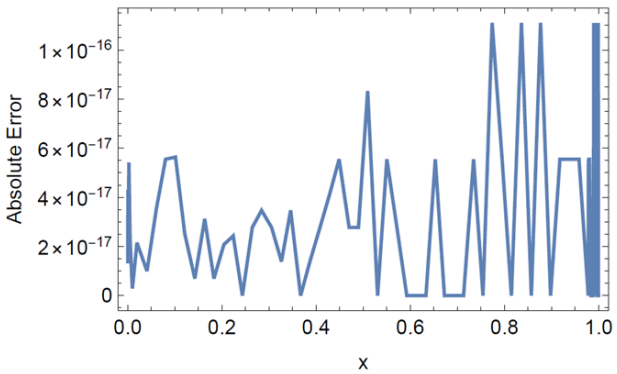

Figure 3. AE via $N = 4$, $\alpha = 0.8$, and $\beta = 1.4$ for Example 2

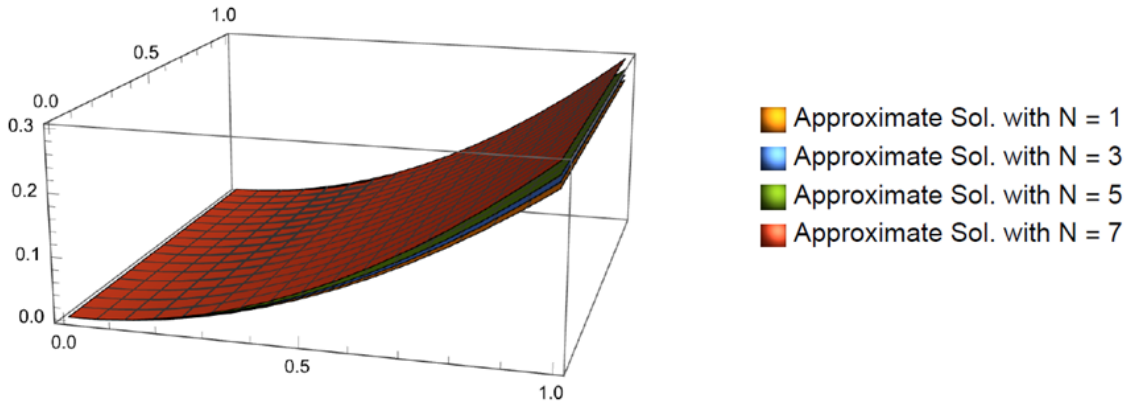

Figure 4. Approximate solution via different values of N for Example 2

Example 3 (Cubic-Quintic-Heptic nonlinear polynomial models [23])**.** Consider the following nonlinear equation with constraints $v(0) = 1$, $v'(0) = 0$

$$D^{\alpha}v(x) + f\,D^{\beta}v(x) + h\,v(x) + c\,v^3(x) + m\,v^5(x) + e\,v^7(x) = g(x), \quad x \in [0,1]. \tag{31}$$

The analytic solution is $v(x) = 1 + x^3$. We note that since the exact solution $v(x) = 1 + x^3$ is a polynomial of degree 3, it is exactly contained in the approximation space for $N \geq 1$. Thus, the machine-level accuracy observed here demonstrates the polynomial exactness of the method, serving as a successful verification of the implementation. The invariant error across different nonlinear cases is a consequence of the solution being exactly represented in the basis, with the residual error dominated by the fixed machine precision limit of the arithmetic operations rather than the nonlinearity itself. For the integer-order limiting cases, the fractional orders are assigned the values $\alpha = 2$, $\beta = 1$, and $N = 3$. We investigate three distinct integer-order case studies associated with Example 3:

Case I. f = 2, h = 1, c = 8 , m = 0, e = 0 (Cubic Nonlinearity).
Case II. f = 2, h = 1, c = 8 , m = 2, e = 0 (Cubic-Quintic Nonlinearity).
Case III. f = 2, h = 1, c = 8 , m = 2, e = 3 (Cubic-quintic-Heptic Nonlinearity).

Table 5. Comparison of absolute errors for Example 3 at N = 3

Case	I		II		III	
x	Our method	Method in [23]	Our method	Method in [23]	Our method	Method in [23]
0.1	1.06035×10^{-16}	2.54144×10^{-18}	1.06035×10^{-16}	1.65877×10^{-17}	1.06035×10^{-16}	3.87176×10^{-18}
0.2	1.73472×10^{-17}	6.61306×10^{-18}	1.06035×10^{-16}	5.70251×10^{-17}	1.06035×10^{-16}	1.45989×10^{-17}
0.3	8.32667×10^{-17}	6.88578×10^{-18}	1.06035×10^{-16}	1.07323×10^{-16}	1.06035×10^{-16}	3.08491×10^{-17}
0.4	6.93889×10^{-17}	1.96947×10^{-18}	1.06035×10^{-16}	1.53493×10^{-16}	1.06035×10^{-16}	5.12900×10^{-17}
0.5	1.38778×10^{-17}	2.52818×10^{-17}	1.06035×10^{-16}	1.81547×10^{-16}	1.06035×10^{-16}	7.45896×10^{-17}
0.6	0	6.83802×10^{-17}	1.06035×10^{-16}	1.77494×10^{-16}	1.65877×10^{-16}	9.94154×10^{-17}
0.7	5.55112×10^{-17}	1.36594×10^{-16}	1.06035×10^{-16}	1.27348×10^{-16}	1.06035×10^{-16}	1.24435×10^{-16}
0.8	0	2.35252×10^{-16}	1.06035×10^{-16}	1.71176×10^{-17}	1.06035×10^{-16}	1.48317×10^{-16}
0.9	1.11022×10^{-16}	3.69683×10^{-16}	1.06035×10^{-16}	1.67184×10^{-16}	1.06035×10^{-16}	1.69728×10^{-16}

Table 5 presents a comparative analysis of the absolute errors obtained via the proposed method and the technique developed in [23] for $N = 3$, $\alpha = 2$, and $\beta = 1$. A closer inspection of the numerical data reveals that both approaches achieve exceptional precision, with the AEs consistently remaining within the order of 10^{-16} to 10^{-18}. In Case (I), the proposed method exhibits highly competitive accuracy; notably, the error completely vanishes (yielding an exact absolute error of zero) at specific nodes such as $x = 0.6$ and $x = 0.8$, underscoring its superior localized convergence properties. Furthermore, for Cases (II) and (III), the proposed algorithm demonstrates remarkable stability, maintaining a uniform AE of approximately 1.06035×10^{-16} across nearly all spatial nodes. In contrast to the fluctuations observed in the results of [23], the steady and invariant error profile of the present method highlights its robust performance and geometric consistency when handling

highly nonlinear terms, such as cubic-quintic and cubic-quintic-septic structures. Figure 5 shows the absolute error via $N = 4$, $\alpha = 2$, and $\beta = 1$.

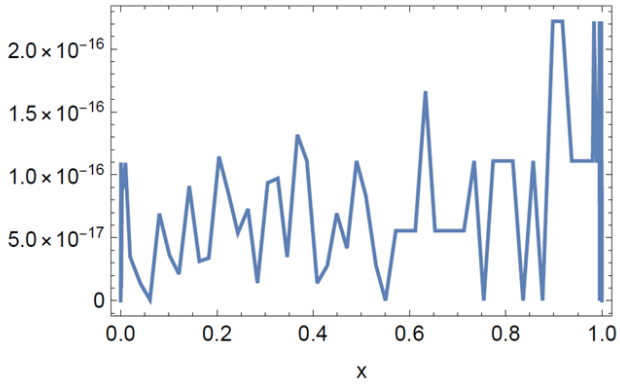

Figure 5. Absolute error via $N = 4$, $\alpha = 2$, and $\beta = 1$ for Example 3

Example 4 (Generalized Liénard equation via hyperbolic solutions [24–26])**.** We investigate a highly nonlinear Liénard equation explicitly formulated as $v''(x) + (\beta_1 + \beta_2 v^2(x))v'(x) + \beta_3 v(x) + \beta_4 v^3(x) = 0$, which maps to the generic form with $\alpha = 2, \beta = 0$ and specific nonlinear coefficients:

$$D^{\alpha} v(x) + f\, D^{\beta} v(x) + h\, v(x) + c\, v^3(x) + m\, v^5(x) + e\, v^7(x) = g(x), \quad x \in [0,1], \tag{32}$$

subject to $v(0) = \frac{1}{\sqrt{2}}$, $v'(0) = \frac{\sqrt{2}}{4}$. The analytic solution is $v(x) = \sqrt{\frac{1+\tanh(x)}{2}}$.

Table 6 presents a comparative validation of the absolute errors (AEs) against three established numerical methods: the differential transform method, a hybrid heuristic computational approach, and an accurate Liénard-solver proposed in [24], [25], and [26]. Operating at a mere fraction of the basis size (N = 6 in the reference literature), the proposed scheme attains an absolute error bound of 10^{-17}, outperforming the reference models by up to eleven orders. Figure 6 shows the approximate error at $N = 6$, $\alpha = 2$, and $\beta = 0$. Figure 7 shows the multi-component approximate solutions mapped via different values of N.

Table 6. Comparison of AEs of Example 4 at $\alpha = 2$ and $\beta = 0$

x	Our method	Method in[25]	Method in[26]	Method in[24]
	N = 6	N = 6	N = 6	N = 6
0.1	6.78711×10^{-17}	2.2683×10^{-6}	6.24×10^{-6}	6.7141×10^{-8}
0.2	8.06646×10^{-17}	2.5222×10^{-6}	5.60×10^{-6}	1.1401×10^{-7}
0.3	1.9082×10^{-17}	1.4404×10^{-5}	5.15×10^{-6}	1.4010×10^{-7}
0.4	7.28584×10^{-17}	6.1806×10^{-5}	5.08×10^{-6}	1.4855×10^{-7}
0.5	2.08167×10^{-17}	2.2099×10^{-4}	5.00×10^{-6}	1.4131×10^{-7}
0.6	1.249×10^{-16}	6.5187×10^{-4}	4.60×10^{-6}	2.6414×10^{-7}
0.7	6.93889×10^{-18}	1.6408×10^{-3}	3.96×10^{-6}	4.3610×10^{-7}
0.8	1.38778×10^{-17}	3.6469×10^{-3}	3.39×10^{-6}	5.8126×10^{-7}
0.9	1.38778×10^{-17}	7.3493×10^{-3}	3.15×10^{-6}	6.4934×10^{-7}

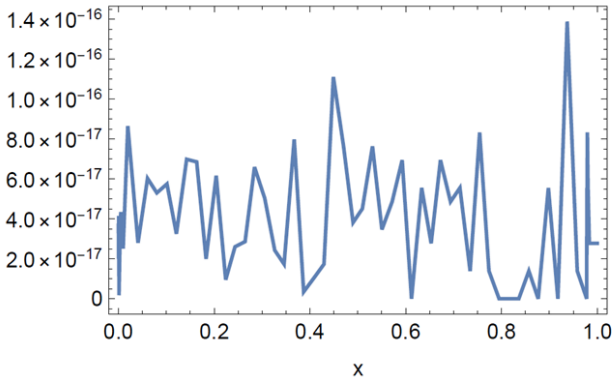

Figure 6. AE via $N = 6$, $\alpha = 2$, and $\beta = 0$ for Example 4

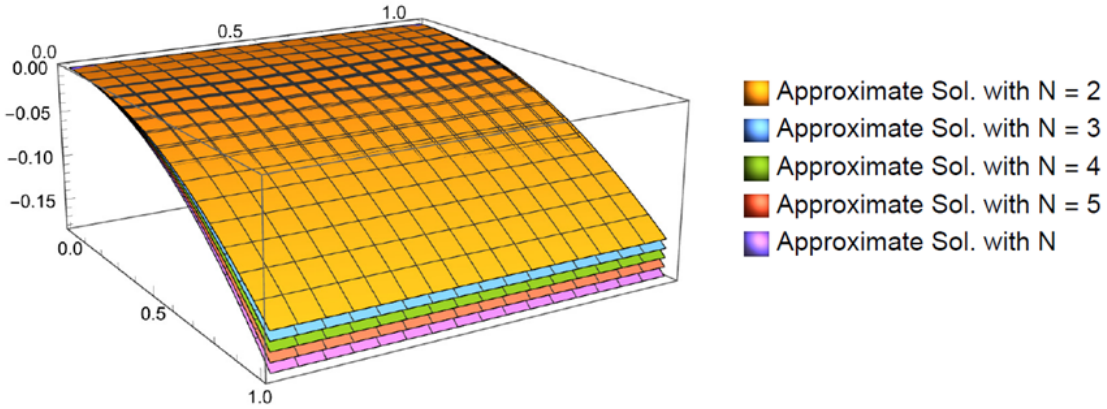

Figure 7. Approximate solution via various values of N, $\alpha = 2$, and $\beta = 0$ for Example 4

Example 5 (Highly nonlinear boundary-layer Liénard system)**.** For rigorous test case, we consider a Liénard formulation explicitly defined with its nonlinear functions $f(y)$ and $g(y)$ featuring complex irrational coefficients [24–26]:

$$D^{\alpha}v(x) + f\,D^{\beta}v(x) + h\,v(x) + c\,v^3(x) + m\,v^5(x) + e\,v^7(x) = g(x), \quad x \in [0,1], \tag{33}$$

subjected to $v(0) = \frac{1}{\sqrt{1+\sqrt{2}}}$, $v'(0) = 0$. The exact solution is given by the hyperbolic function:

$$v(x) = \sqrt{\frac{\operatorname{sech}^2(x)}{2\sqrt{2} + (1-\sqrt{2})\operatorname{sech}^2(x)}}. \tag{34}$$

Table 7 verifies the absolute errors under $N = 3$, $\alpha = 2$, and $\beta = 0$. The proposed Delannoy collocation algorithm achieves an error range of 10^{-17}, significantly surpassing the precision scales of $10^{-2} \approx 10^{-6}$ recorded by alternative methods in [24–26]. Lastly, Table 8 chronicles the relationship between the exact solution, the computed approximate fields, and the corresponding AEs for higher-order expansions (N = 4 and N = 5), validating the structural stability and rapid spectral convergence of our numerical scheme. The spatial distribution of the absolute error for N = 3, $\alpha = 2$, and $\beta = 0$ is illustrated in Figure 8.

Table 7. Comparison of AEs of Example 5 at $\alpha = 2$ and $\beta = 0$

x	Our method	Method in [25]	Method in [26] (Interior Point Algorithm)	Method in [26] (Active Set Algorithm)	Method in [24]
	N = 3	N = 4	N = 4	N = 4	N = 4
0.1	4.0332×10^{-17}	4.0668×10^{-6}	4.33×10^{-5}	1.64×10^{-5}	2.5685×10^{-8}
0.2	4.3368×10^{-17}	3.7000×10^{-6}	5.31×10^{-5}	2.22×10^{-5}	5.1433×10^{-7}
0.3	1.3878×10^{-17}	7.1793×10^{-6}	5.84×10^{-5}	2.55×10^{-5}	1.3397×10^{-6}
0.4	4.1633×10^{-17}	6.1806×10^{-5}	6.37×10^{-5}	2.21×10^{-5}	2.3254×10^{-6}
0.5	1.3878×10^{-17}	2.4676×10^{-4}	6.49×10^{-5}	1.54×10^{-5}	3.2340×10^{-6}
0.6	1.3878×10^{-17}	9.9922×10^{-4}	6.01×10^{-5}	1.11×10^{-5}	3.8973×10^{-6}
0.7	0	3.2168×10^{-3}	5.27×10^{-5}	1.09×10^{-5}	4.2577×10^{-6}
0.8	0	8.7371×10^{-3}	4.67×10^{-5}	1.13×10^{-5}	4.3703×10^{-6}
0.9	5.5511×10^{-17}	2.0841×10^{-2}	4.28×10^{-5}	7.47×10^{-6}	4.3323×10^{-6}

Table 8. Comparison for Example 5 at $\alpha = 2$ and $\beta = 0$

		$N = 4$		$N = 5$	
x	Exact Sol.	Approximate Sol.	Absolute Error	Approximate Sol.	Absolute Error
0.1	0.00374953	0.00374953	3.72966×10^{-17}	0.00374953	1.07336×10^{-15}
0.2	0.0147514	0.0147514	5.37764×10^{-17}	0.0147514	2.9126×10^{-15}
0.3	0.0322654	0.0322654	0	0.0322654	4.56579×10^{-15}
0.4	0.055058	0.055058	6.245×10^{-17}	0.055058	6.39072×10^{-15}
0.5	0.0814022	0.0814022	0	0.0814022	8.18789×10^{-15}
0.6	0.109077	0.109077	5.55112×10^{-17}	0.109077	1.0103×10^{-14}
0.7	0.13537	0.13537	0	0.13537	1.21292×10^{-14}
0.8	0.157072	0.157072	5.55112×10^{-17}	0.157072	1.48215×10^{-14}
0.9	0.170483	0.170483	5.55112×10^{-17}	0.170483	1.82077×10^{-14}
1	0.171408	0.171408	2.77556×10^{-17}	0.171408	1.98175×10^{-14}

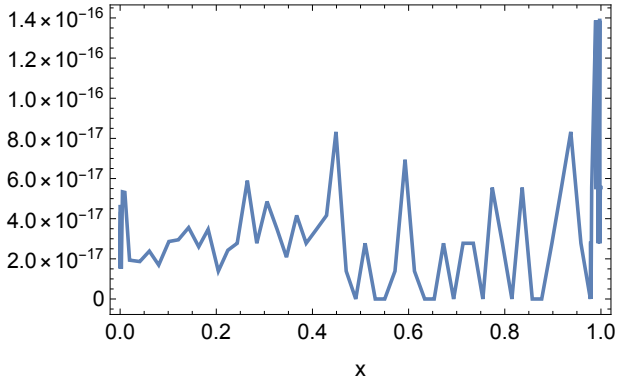

Figure 8. AE via $N = 3$, $\alpha = 2$, and $\beta = 0$ for Example 5

6. Conclusion and outlook

In this work, a highly efficient and accurate spectral collocation method based on Delannoy polynomials was successfully developed to solve nonlinear fractional diffusion-type and Liénard ordinary differential equations. By constructing the operational matrices for the Caputo fractional derivative, the governing differential equations were efficiently converted into a system of algebraic equations. Numerical simulations across several benchmark examples demonstrated that the proposed method converges rapidly and achieves high precision (often reaching machine precision limits) with a moderate number of basis functions. Comparative analyses against existing techniques confirmed that the Delannoy framework delivers highly competitive and often more accurate results under comparable settings. Ultimately, these results establish

Delannoy polynomials as a powerful, robust, and computationally economical alternative to classical polynomial bases for solving complex fractional-order systems in physics and engineering.

Conflicts of Interest: The authors declare no conflict of interest.

Data Availability: No data is required for this research.

Funding Information: No funding is available for this research.

Acknowledgments: The authors thanks the reviewers and the editor for their careful reading and valuable comments and suggestions.

References

[1] Strogatz, S. H. (2018). *Nonlinear Dynamics and Chaos: With Applications to Physics, Biology, Chemistry, and Engineering* (2nd ed.). CRC Press.

[2] Perko, L. (2001). *Differential Equations and Dynamical Systems* (3rd ed.). Springer.

[3] Hirsch, M. W., Smale, S., & Devaney, R. L. (2012). *Differential Equations, Dynamical Systems, and an Introduction to Chaos* (3rd ed.). Academic Press.

[4] Liénard, A. (1928). Étude des oscillations entretenues. *Revue Générale de l'Électricité, 23*, 901–912, 946–954.

[5] Nayfeh, A. H., & Mook, D. T. (2008). *Nonlinear Oscillations*. Wiley.

[6] Kovacic, I., & Brennan, M. J. (Eds.). (2011). *The Duffing Equation: Nonlinear Oscillators and Their Behaviour*. Wiley.

[7] Caputo, M. (1967). Linear models of dissipation whose Q is almost frequency independent—II. *Geophysical Journal International, 13*(5), 529–539.

[8] Podlubny, I. (1999). *Fractional Differential Equations: An Introduction to Fractional Derivatives, Fractional Differential Equations, to Methods of Their Solution and Some of Their Applications*. Academic Press.

[9] Mainardi, F. (2010). *Fractional Calculus and Waves in Linear Viscoelasticity: An Introduction to Mathematical Models*. World Scientific.

[10] Shen, J., Tang, T., & Wang, L.-L. (2011). *Spectral Methods: Algorithms, Analysis and Applications*. Springer.

[11] Canuto, C., Hussaini, M. Y., Quarteroni, A., & Zang, T. A. (2006). *Spectral Methods: Fundamentals in Single Domains*. Springer.

[12] Sayed, S. M., Mohamed, A. S., Abo El-Dahab, E. M., & Youssri, Y. H. (2024). Alleviated shifted Gegenbauer spectral method for ordinary and fractional differential equations. *Contemporary Mathematics, 5*(2), 1344–1370.

[13] Sayed, S. M., Mohamed, A. S., Abo-Eldahab, E. M., & Youssri, Y. H. (2025). A compact combination of second-kind Chebyshev polynomials for Robin boundary value problems and Bratu-type equations. *Journal of Umm Al-Qura University for Applied Sciences, 11*, 766–783.

[14] Kamel, S. G., Atta, A. G., & Youssri, Y. H. (2025). An explicit spectral tau method with Delannoy polynomials for the time-fractional diffusion equation. *Open Journal of Mathematical Analysis, 9*(2), 134–144.

[15] Youssri, Y. H. (2017). A new operational matrix of Caputo fractional derivatives of Fermat polynomials: An application for solving the Bagley–Torvik equation. *Advances in Difference Equations, 2017*, 73.

[16] Sun, Z.-W. (2018). Arithmetic properties of Delannoy numbers and Schröder numbers. *Journal of Number Theory, 183*, 146–171.

[17] Wang, Y., Zheng, S.-N., & Chen, X. (2019). Analytic aspects of Delannoy numbers. *Discrete Mathematics, 342*(8), 2270–2277.

[18] Youssri, Y. H., Basha, S. H., & Atta, A. G. (2026). A Delannoy polynomial-based collocation framework for solving nonlinear fourth-order integro-differential equations. *Journal of Applied Mathematics and Computing, 72*, 81.

[19] Baleanu, D., Diethelm, K., Scalas, E., & Trujillo, J. J. (2012). *Fractional Calculus: Models and Numerical Methods*. World Scientific.

[20] Dumortier, F., Llibre, J., & Artés, J. C. (2006). *Qualitative Theory of Planar Differential Systems*. Springer.

[21] Pirmohabbati, P., Refahi Sheikhani, A. H., Saberi Najafi, H., & Abdolahzadeh Ziabari, A. (2020). Numerical solution of full fractional Duffing equations with cubic–quintic–heptic nonlinearities. *AIMS Mathematics, 5*(2), 1621–1641.

[22] Abd-Elhameed, W. M., Alqubori, O. M., Amin, A. K., & Atta, A. G. (2025). Numerical solutions for nonlinear ordinary and fractional Duffing equations using combined Fibonacci–Lucas polynomials. *Axioms, 14*(4), 314.

[23] El-Sayed, A. A. E. (2023). Pell–Lucas polynomials for numerical treatment of the nonlinear fractional-order Duffing equation. *Demonstratio Mathematica, 56*(1), 20220220.

[24] Kiltu, G. G., & Duressa, G. F. (2019). Accurate numerical method for Liénard nonlinear differential equations. *Journal of Taibah University for Science, 13*(1), 740–745.

[25] Matinfar, M., Bahar, S. R., & Ghasemi, M. (2012). Solving the Liénard equation by differential transform method. *World Journal of Modelling and Simulation, 8*(2), 142–146.

[26] Malik, S. A., Qureshi, I. M., Amir, M., & Haq, I. U. (2013). Numerical solution of Liénard equation using hybrid heuristic computation. *World Applied Sciences Journal*, *28*(5), 636–643.